N84-27832

SIMPLIFIED COMPOSITE MICROMECHANICS EQUATIONS FOR STRENGTH, FRACTURE TOUGHNESS, IMPACT RESISTANCE AND ENVIRONMENTAL EFFECTS

Lewis Research Center
Cleveland, OH

1984

U.S. DEPARTMENT OF COMMERCE
National Technical Information Service
NTIS®

NASA Technical Memorandum 83696

Simplified Composite Micromechanics Equations for Strength, Fracture Toughness, Impact Resistance and Environmental Effects

C. C. Chamis
Lewis Research Center
Cleveland, Ohio

Prepared for the
~~Twenty-ninth~~ Annual Conference of the
Society of the Plastics Industry (SPI)
Reinforced Plastics/Composites Institute
Houston, Texas, January 16-20, 1984

NASA

1. Report No.	2. Government Accession No.	3. Recipient's Catalog No.
NASA TM-83696		

4. Title and Subtitle	5. Report Date
Simplified Composite Micromechanics Equations for Strength, Fracture Toughness and Environmental Effects	6. Performing Organization Code: 505-33-5B

7. Author(s)	8. Performing Organization Report No.
C. C. Chamis	E-2154
	10. Work Unit No.

9. Performing Organization Name and Address	11. Contract or Grant No.
National Aeronautics and Space Administration Lewis Research Center Cleveland, Ohio 44135	13. Type of Report and Period Covered: Technical Memorandum
12. Sponsoring Agency Name and Address	14. Sponsoring Agency Code
National Aeronautics and Space Administration Washington, D.C. 20546	

15. Supplementary Notes

Prepared for the Thirty-ninth Annual Conference of the Society of the Plastics Industry (SPI) Reinforced Plastics/Composites Institute, Houston, Texas, January 16-20, 1984.

16. Abstract

A unified set of composite micromechanics equations of simple form is summarized and described. This unified set includes composite micromechanics equations for predicting (1) ply in-plane uniaxial strengths; (2) through-the-thickness strength (interlaminar and flexural); (3) in-plane fracture toughness; (4) in-plane impact resistance; and (5) through-the-thickness (interlaminar and flexural) impact resistance. Equations are also included for predicting the hygrothermal effects on strength, fracture toughness and impact resistance. Several numerical examples are worked out to illustrate the ease of use of the various composite micromechanics equations. The numerical examples were selected, in part, to demonstrate the interrelationships of the various constituent properties in composite strength and strength-related behavior, to make comparisons with available experimental data and to provide insight into composite strength behavior.

17. Key Words (Suggested by Author(s))	18. Distribution Statement
Fiber composite; Micromechanics; Uniaxial strengths; Flexural; Fracture toughness; Impact resistance; Environmental effects; Predictions; Numerical examples	Unclassified - unlimited STAR Category 24

19. Security Classif. (of this report)	20. Security Classif. (of this page)	21. No. of pages	22. Price*
Unclassified	Unclassified		

*For sale by the National Technical Information Service, Springfield, Virginia 22161

SIMPLIFIED COMPOSITE MICROMECHANICS EQUATIONS FOR STRENGTH, FRACTURE TOUGHNESS, IMPACT RESISTANCE AND ENVIRONMENTAL EFFECTS

C. C. Chamis*
National Aeronautics and Space Administration
Lewis Research Center
Cleveland, Ohio 44135

SUMMARY

A unified set of composite micromechanics equations of simple form is summarized and described. This unified set includes composite micromechanics equations for predicting (1) ply in-plane uniaxial strengths; (2) through-the-thickness strength (interlaminar and flexural); (3) in-plane fracture toughness; (4) in-plane impact resistance; and (5) through-the-thickness (interlaminar and flexural) impact resistance. Equations are also included for predicting the hygrothermal effects on strength, fracture toughness and impact resistance. Several numerical examples are worked out to illustrate the ease of use of the various composite micromechanics equations. The numerical examples were selected, in part, to demonstrate the interrelationships of the various constituent properties in composite strength and strength-related behavior, to make comparisons with available experimental data and to provide insight into composite strength behavior.

INTRODUCTION

The several strengths (stresses at fracture) of unidirectional composites are fundamental to analysis/design of fiber composite structures. Some of these strengths are determined by physical experiments. Others are not easily amenable to direct measurement by testing. In addition, testing is usually time consuming, costly, and the composite must have been made prior to testing. Furthermore, parametric studies of the effects of fiber volume ratio on properties such as impact resistance and fracture toughness can only be made by an extensive combination of tests. Another approach is the use of composite micromechanics to derive equations for predicting composite strengths based on constituent (fiber and matrix) properties. Over the last twenty years, composite micromechanics has been used to derive equations for predicting selected composite strengths (ref. 1). However, these equations are not readily available since equations for different strengths are scattered throughout the literature.

Herein, a unified set of composite micromechanics equations is summarized and described. The set includes simple equations for predicting ply (unidirectional composite) strengths using constituent properties. Equations are for: (1) tensile strengths (in-plane and through-the-thickness), (2) flexural strength, (3) impact resistance, and (4) fracture toughness. Also, equations are presented for the effects of (1) moisture, and (2) temperature. Results predicted by these equations are compared with available experimental data.

---

*Aerospace Structures and Composites Engineer.

These data are primarily from Refs. 1 to 5. The equations are summarized in subsets corresponding to related strengths such as in-plane, through-the-thickness, etc. The description consists of the significance of the participating variables in the equations of each subset, several numerical examples and possible implications.

The equations of each subset (strengths, fracture toughness, impact resistance and hygorthermal degradation effects) are summarized in chart form (labeled figures). This allows the equations for each subset to be in one page for convenience of use and identification of interrelationships. Constituent material properties used in the numerical examples are tabulated and identified with the same symbol used in the equations. The numerical examples are presented in narrative form, rather than tabular, in order to conserve space. The symbols used are summarized in the Appendix for convenience of reference.

Many of the equations included in this composite micromechanics unified set appear in their present simplified form for the first time. These equations evolved from continuing research on composite micromechanics and composite computational mechanics at Lewis Research Center. Also, this is the first unified set which provides a quantified description of composite strength and strength-related behavior (fracture toughness and impact resistance) at the micromechanistic level.

SYMBOLS

c	heat capacity
D	diffusivity
d	diameter
E	modulus of elasticity
G	shear modulus
	impact energy density
K	heat conductivity
k	volume ratio
M	moisture - percent by weight
N_f	number of filaments per roving end
P	property
RHR	relative humidity ratio
S	strength
$\mathcal{S}$	fracture "toughness"
T	temperature
t	thickness
x,y,z	structural reference axes
1,2,3	ply material axes
α	thermal expansion coefficient
β	moisture expansion coefficient

δ	interfiber, interply spacing
ξ	fracture strain, strain
θ	ply orientation angle
λ	weight percent
ρ	density
σ	stress

Subscripts:

F	fiber property
C	compression property
D	dry property
G	glass-transition
F	flexural
ℓ	ply property
m	matrix property
S	shear
SB	short beam shear
T	tension
v	void
W	wet
o	reference property, temperature
∞	saturation
1,2,3	direction corresponding to 1,2,3 ply material axes

COMPOSITE MECHANICS -- DEFINITIONS AND CONSTITUENT MATERIALS

The branch of composite mechanics which provides the formal structure to relate ply uniaxial strengths to constituent properties is called composite micromechanics. Composite micromechanics for uniaxial strengths is identified concisely in the schematic in figure 1. The schematic in this figure defines the inputs to composite micromechanics and the outputs. The inputs consist of constituent material (fiber/matrix) properties, geometric configuration, environmental conditions, and the fabrication process. The outputs consist of ply uniaxial strengths, impact resistance, fracture toughness and hygrothermal effects.

The formal structure of composite micromechanics (concepts, math-models and equations) is developed based on certain assumptions (consistent with the physical situation) and the principles of solid mechanics. The four main assumptions made in deriving the equations described herein are: (1) the ply resists loads as depicted schematically in figure 2; (2) the ply and its constituents behave linearly elastic to fracture as is illustrated in figure 3; (3) the ply uniaxial strengths are associated with their respective fracture modes shown in figure 4; and (4) there is complete bond at the interface of the constituents. Though the principles of solid mechanics can be used with

various levels of mathematical sophistication, the mechanics of materials was used in deriving the equations summarized herein because it leads to explicit equations of simple form for each property.

Properties along the fiber direction (1-axis, fig. 2) are conventionally called longitudinal; those transverse to the fiber direction (2-axis, fig. 2) are called transverse; the in-plane shear is also called intralaminar shear (1-2 plane, fig. 2). Those through the thickness (3-axis, fig. 2) are called interlaminar properties. All ply properties are defined with respect to the ply material axes denoted by 1, 2 and 3 in figure 2 for description/analysis purposes. Most ply properties are denoted by a letter with suitable subscripts. The subscripts are selected to identify type of property (ply, fiber, matrix), plane, direction, and sense in the case of strengths. For example, $S_{\ell 11T}$ denotes ply longitudinal tensile strength while S_{fT} denotes fiber tensile strength. Though this notation may seem cumbersome, it is necessary to properly differentiate among the multitude of ply and constituent properties.

A variety of fibers have been used to make composites. Some of these are summarized in table 1 with their respective properties needed for composite micromechanics. Similarly, some typical matrix resins are summarized in table 2.

UNIAXIAL STRENGTHS -- IN-PLANE

There are five in-plane ply uniaxial strengths. These are identified as: (1) longitudinal tension ($S_{\ell 11T}$); (2) longitudinal compression ($S_{\ell 11C}$); (3) transverse tension ($S_{\ell 22T}$); (4) transverse compression ($S_{\ell 22C}$); and (5) in-plane or intralaminar shear ($S_{\ell 12S}$). The fracture modes associated with each uniaxial strength are depicted schematically in figure 4. Note that there are three different and distinct fracture modes for longitudinal compression (fig. 4-b): (1) fiber compression (shear plane) fracture; (2) delamination transverse splitting or panel buckling; and (3) fiber microbuckling.

The composite micromechanics equations for the ply uniaxial strengths are summarized in figure 5 with attendant schematics. The schematics define the load direction, fiber orientation and the notation used in the micromechanics equations. The first five equations describe the in-plane uniaxial strengths, respectively: $S_{\ell 11T}$, $S_{\ell 11C}$, $S_{\ell 22T}$, $S_{\ell 22C}$, and $S_{\ell 12S}$. The last equation is for the void effect on the resin strength (S_m) and also provides lower bound estimates on $S_{\ell 22T}$, $S_{\ell 22C}$ and $S_{\ell 12S}$ as will be described later.

The following are observed from the micromechanics equations for ply uniaxial strengths: (1) $S_{\ell 11T}$ depends on S_{fT} and the fiber compression fracture mode for $S_{\ell 11C}$ depends on S_{fC}. These are the only two that are fiber strength dominated. (2) The delamination/splitting for $S_{\ell 11C}$ depends on matrix shear strength (through $S_{\ell 12S}$ (eq. 5)) and the matrix tensile strength and, therefore, is resin strength dominated. (3) The microbuckling fracture mode for $S_{\ell 11C}$ depends strongly on the shear modulus and mildly on the modular ratio (G_m/G_{f12}) and, therefore, is resin stiffness dominated. (4) The other three ($S_{\ell 22T}$, $S_{\ell 22C}$ and $S_{\ell 12S}$) depend strongly on the respective resin strengths and are, therefore, resin strength dominated. (5) The fiber volume ratio affects strongly $S_{\ell 11T}$ and $S_{\ell 11C}$ (fiber compressing or fiber microbuckling) which are the fiber strength or shear stiffness dominated ply strengths). (6) The fiber volume ratio affects mildly $S_{\ell 22T}$, $S_{\ell 22T}$, $S_{\ell 22C}$, $S_{\ell 12S}$ and $S_{\ell 11C}$ (delamination/

shear) which are the resin-strength dominated ply uniaxial strengths. (7) The voids influence the matrix strength. Several examples below illustrate use of the uniaxial strength equations in figure 5.

Example 3.1. Calculate the ply tensile strength ($S_{\ell 11T}$) of a graphite fiber (AS)/intermediate modulus, high strength (IMHS) epoxy (AS/E) composite with 0.6 fiber volume ratio. From table 1, S_{ft} = 350 ksi and from equation (1) (fig. 5), $S_{\ell 11T}$ = 210 ksi which is the same as the measured value in table 3.

Example 3.2. Calculate the ply compression strength for an AS/E (IMHS) composite with 0.6 fiber volume ratio. All three equations (eq. (2), fig. 5) should be used. To use the first equation, S_{fc} must be known. If it is not known, $S_{fc} \approx 0.9\ S_{fT}$ is a good approximation for graphite fiber/matrix composites (ref. 6). Using this approximation and respective values for tables 1 and 2 in equation (2) figure 5 from the first equation:

$S_{\ell 11C}$ = 0.6 x 0.9 x 350 = 189 ksi

from the second equation (note need evaluate $S_{\ell 12S}$ from eq. (5), example 3.5 with incomplete bond)

$S_{\ell 11C}$ = 10.0 x 8.1 + 2.5 x 15 = 118 ksi

from the third equation,

$S_{\ell 11C}$ = 0.185/[1.0-0.6 (1.0-0.185/2.0)] = 406 ksi

A conservative approach is to select the lowest value or $S_{\ell 11C}$ = 118 ksi. This is about 69 percent of the typical measured value of 170 ksi in table 3. The value of 189 ksi predicted by the first equation is also reasonable. This value could be used in laminates which have other than 0° plies on the outside.

Example 3.3. Calculate the ply transverse tensile strength ($S_{\ell 22T}$) for an AS/E (IMHS) composite with 0.6 fiber volume ratio. From equation (3) and respective values from tables 1 and 2

$S_{\ell 22T} = [1.0 - (\sqrt{0.6} - 0.6) \times (1.0 - 0.5/2.0)] \times 15 = 13$ ksi

This is about twice the measured value of 7 ksi in table 3. One major reason for this difference is the complete bond at the fiber/matrix interface assumed in deriving equation (3), figure 5. Incomplete bond at the interface may be approximated by assuming the presence of voids. Assuming about 5 percent voids by volume (k_v = 0.05) and using equation (6) (fig. 5), the reduced or degraded resin tensile strength

$$S_{mT} = \left\{1.0 - [4\ (0.05)/(1.0-0.6)\ \pi]^{1/2}\right\} \times 15 = 9.0 \text{ ksi}$$

Using this reduced resin strength in equation (3) (fig. 5) $S_{\ell 22T}$ = 7.8 ksi which is a reasonable estimation compared to the measured value of 7 ksi.

The above calculations lead to the conclusion that estimation of $S_{\ell 22T}$, then, requires two steps:

1. Degradation of S_{mT} due to 5 percent voids by volume (k_v = 0.05) as predicted by equation 6 (fig. 5).
2. Substitution of the degraded S_{mT} in equation (3).

Though the value of 5 percent voids may seem somewhat arbitrary, it is reasonable since equation (3), figure 5, does not account for factors such as

nonuniform fiber distribution within the ply, incomplete (partial) bond at the fiber/matrix interface, and possible differences in the in situ resin matrix properties compared to the neat resin properties.

Example 3.4. Calculate the transverse compression strength ($S_{\ell 22C}$) for an AS/E (IMHS) with 0.6 fiber volume ratio. From equation (4) and respective values from tables 1 and 2

$S_{\ell 22C} = [1.0 - (\sqrt{0.6} - 0.6)\ (1.0 - 0.5/2.0)] \times 35.0 = 30.4$ ksi

This values is about 85 percent of the typical value in table 3. It is worth noting that the interfacial bond and fiber nonuniformity are not critical in transverse compression and, therefore, do not contribute to resin compression strength degradation.

Example 3.5. Calculate the intralaminar shear strength ($S_{\ell 12S}$) for an AS/E (IMHS) with 0.6 fiber volume ratio. From equation (5) and respective values from tables 1 and 2

$S_{\ell 12S} = [1.0 - (\sqrt{0.6} - 0.6)\ (1.0 - 0.185/2.0)] \times 13 = 10.9$ ksi

This values is about 21 percent greater than the typical measured value 9 ksi, table 3. This value is reasonable in view of the nonuniform fiber distribution bonding condition at the interface and deviations in in situ properties from neat resin properties as was mentioned for $S_{\ell 22T}$ (example 3.2). A closer estimate to the measured value may be obtained by degrading the matrix shear strength S_{mS} assuming 2 percent voids ($k_v = 0.02$) in equation (6), figure 5. The result is $S_{\ell 12S} = 8.1$. It is worth noting that the various factors that affect the transverse tensile strength also affect the intralaminar shear strength but not as severely.

Example 3.6. Calculate the effect of voids on the ply transverse tensile strength of an AS/E (IMHS) with 0.6 fiber volume ratio ($k_f = 0.6$) and 0.02 void volume ratio ($k_v = 0.02$). This is accomplished using the following three steps:

1. Voids effect on S_{mT} (eq. (6), fig. 5).
   $S_{mT} = \{1.0 - [4(0.02)/(1.0 - 0.6)\ \pi]^{1/2}\} \times 15 = 11.2$ ksi
2. Incomplete interfacial bond effects
   $S_{mT} = \{1.0 - [4\ (0.05)/(1.0 - 0.6\ \pi]^{1/2}\} \times 11.2 = 6.8$ ksi
3. Transverse tensile strength (eq. (3), fig. 5)
   $S_{\ell 22T} = [1.0 - (\sqrt{0.6} - 0.6)\ (1 - 0.5/2.0)]\ 6.8 = 5.9$ ksi

Note that the two void ratios ($k_v = 0.02$ and $k_v = 0.05$) are not additive since equation (6) is nonlinear.

Example 3.7. Calculate the lower bound of the ply transverse tensile strength for an AS/E (IMHS) composite with $k_f = 0.6$. For this case, we use equation (6), figure 5, with: $k_v = 0.6$, $k_f = 0.0$ and $S_{\ell 22T} = S_m$.

$S_{\ell 22T} = \{1.0 - [4\ (0.6)/\pi]^{1/2}\} \times 15 = 1.9$ ksi

This value is about 27 percent of the typical measured value of 7 ksi and about 15 percent of that predicted by equation (3), figure 5, without any degradation. The lower bound is overly pessimistic for acceptable composites and should be used only by in composites with no interfacial bond. Lower bound

estimates on ply transverse compression ($S_{\ell 22C}$) and ply intralaminar shear strength ($S_{\ell 12S}$) are obtained by following the same procedure.

UNIAXIAL STRENGTHS -- THROUGH-THE-THICKNESS

There are six through-the-thickness uniaxial strengths. These are identified as: (1) longitudinal interlaminar shear (parallel to the fiber direction), ($S_{\ell 13S}$); (2) transverse interlaminar shear (transverse to the fiber direction), ($S_{\ell 23S}$); (3) longitudinal short-beam-shear (parallel to the fiber direction), ($S_{\ell 13SB}$); (4) transverse short-beam-shear (transverse to the fiber direction), ($S_{\ell 23SB}$); (5) longitudinal flexural (bending) ($S_{\ell 11F}$); and (6) transverse flexural ($S_{\ell 22F}$). The composite micromechanics equations for these uniaxial strengths are summarized in figure 6 with attendant schematics. The first six equations describe the six through-the-thickness uniaxial strengths, respectively: $S_{\ell 13S}$, $S_{\ell 23S}$, $S_{\ell 13SB}$, $S_{\ell 23SB}$, $S_{\ell 11F}$ and $S_{\ell 22F}$. The last equation describes the void effects on the resin strength and can also be used as a lower bound on ply strengths dominated by the resin as was mentioned previously.

The following are observed from the composite micromechanics equations in figure 6: (1) $S_{\ell 12S}$ is the same as $S_{\ell 12S}$; (2) $S_{\ell 23S}$ depends strongly on the resin shear strength (S_{mS}) and mildly on k_f and G_m/G_{f23}; (3) the short-beam-shear strengths $S_{\ell 13SB}$ and $S_{\ell 23SB}$ are 1.5 times their respective interlaminar shear strengths ($S_{\ell 13S}$ and $S_{\ell 23S}$); (4) the longitudinal flexural strength ($S_{\ell 11F}$) is fiber dominated and, thus, depends strongly on k_f, s_{fT} and S_{fC}; (5) the transverse flexural strength ($S_{\ell 22F}$) is matrix strength dominated and, thus, depends strongly on S_{mT} and S_{mC} but it depends mildly on k_f and E_m/E_{f22}; (6) the voids degrade matrix strength depending nonlinearly on both k_v and k_f. Several examples below illustrate use of the equations in figure 6.

Example 4.1. Calculate the longitudinal interlaminar shear strength ($S_{\ell 13S}$), for an AS/E (IMHS) composite with 0.6 fiber volume ratio. This is the same as $S_{\ell 12S}$. However, we go through the steps again for completeness. Using equation (4), the first of equation (1), figure 6, and respective property values from tables 1 and 2:

1. Incomplete bond simulation ($k_v = 0.02$)
   $S_{mS} = \{1.0 - [4\ (0.02)/(1.0 - 0.6)\pi]^{1/2}\} \times 13 = 9.7$ ksi
2. Longitudinal interlaminar shear strength
   $S_{\ell 13S} = [1.0 - (\sqrt{0.6} - 0.6)\ (1 - 0.185/2.0)] \times 9.7 = 8.1$ ksi
   which is the same as $S_{\ell 12S}$ as expected.

Example 4.2. Calculate the transverse interlaminar shear strength ($S_{\ell 23S}$) for an AS/E (IMHS) with 0.6 fiber volume ratio. Using S_{mS} from example 4.1, figure 6, and respective properties from table 1 and 2 in the second equation (1), figure 6:

$$S_{\ell 23S} = \left[\frac{1.0 - \sqrt{0.6}\ (1.0 - 0.185/1.0}{1.0 - 0.6\ (1.0 - 0.185/1.0)}\right] \times 9.7 = 7.0 \text{ ksi}$$

Note that $S_{\ell 23S}$ 0.85 $S_{\ell 13S}$ indicating that the ply is weaker in transverse interlaminar shear than in longitudinal interlaminar shear strength.

Example 4.3. Calculate (1) the longitudinal short-beam-shear ($S_{\ell 13SB}$) for the composite in example 4.1; and (2) the transverse short-beam-shear ($S_{\ell 23SB}$) in example 4.2.

1. Using $S_{\ell 13S} = 8.1$ in the first of equation (2), figure 6
   $S_{\ell 13SB} = 1.5 \times 8.1 = 12.1$ ksi
   This value is in reasonably good agreement, under estimating by 14 percent, with the typical measured value of 14 ksi in table 3.
2. Using $S_{\ell 23S} = 7.0$ in the second of equation (2), figure 6
   $S_{\ell 23SB} = 1.5 \times 7.0 = 10.5$ ksi
   Measured values for this strength are not available for comparison.

Example 4.4. Calculate the ply longitudinal flexural strength ($S_{\ell 11F}$) for an AS/E (IMHS) composite with 0.6 fiber volume ratio. Using $k_f = 0.6$, $S_{fC} = 0.9\ S_{fT}$, and $S_{fT} = 350$ ksi (table 1) in the first of equation (3), figure 6.

$$S_{\ell 11F} = \frac{3\ (0.6)\ (350)}{1.0 + 1.0/0.9} = 298 \text{ ksi}$$

This value over estimates the typical measured data of 230 ksi by about 30 percent. A lower estimate for this strength is obtained by using $S_{\ell 11T} = 210$ ksi (from example 3.1) and $S_{\ell 11C} = 118$ ksi (from example 3.2) in the following equation:

$$S_{\ell 11F} = \frac{3\ S_{\ell 11T}}{1 + S_{\ell 11T}/S_{\ell 11C}} = \frac{3 \times 210}{1.0 + 210/118} = 227 \text{ ksi}$$

which estimates the measure value of 230 ksi almost exactly. This is definitely a very good estimate considering the simplicity of the equations and the uncertainties associated with longitudinal compression failure (ref. 6). It also illustrates, in part, that flexural failure is probably a complex combination of tension, compression, and intralaminar shear failures.

Example 4.5. Calculate the ply transverse flexural strength of an AS/E (IMHS) composite with 0.6 fiber volume ratio. Using $k_f = 0.6$ and respective property values from tables 1 and 2 in the second of equation 3.

$$S_{\ell 22F} = \left\{\frac{3\ [1.0 - (\sqrt{0.6} - 0.6)\ (1.0 - 0.5/2.0]}{1.0 + 15/35}\right\} 15 = 27.4 \text{ ksi}$$

This over estimates the typical value of 18 ksi (table 3) by about 52 percent. As was the case for longitudinal flexural strength, a lower estimate can be obtained by substituting $S_{\ell 22T} = 7.8$ ksi (from example 3.3 with partial interfacial bond) and $S_{\ell 22C} = 30.4$ ksi (example 3.4) in the following equation

$$S_{\ell 22F} \quad \frac{3 \times S_{\ell 22T}}{1 + S_{\ell 22T}/S_{\ell 22C}} = \frac{3 \times 7.8}{1.0 + 7.8/30.4} = 18.6 \text{ ksi}$$

which is almost equal to the typical measured values of 18 ksi (table 3).

Example 4.6. Calculate the effect of 3 percent voids on the longitudinal flexural strength for an AS/E (IMHS) with 0.6 fiber volume ratio. The first of equation (3) shows no void effect. However, the lower estimate equation in example (4.4) indicated that the compression strength predicted by the second of equation (3) should be used. This is calculated using the following steps:

1. S_{mS} degraded for voids (eq. (4), fig. 6)
   $S_{mS} = \{1.0 - [4\ (0.03)/(1.0 - 0.6)\ \pi]^{1/2}\} \times 13 = 9.0$ ksi
2. Intralaminar shear strength $S_{\ell 12S}$ (eq. (5), fig. 5) with S_{mS} from step 1.
   $S_{\ell 12S} = [1 - (\ 0.6 - 0.6)\ (1.0 - 0.185/2.0)]\ 9.0 = 7.6$ ksi
3. S_{mT} degraded for voids, void degradation ratio same as in step 1 for S_{mS}
   $S_{mT} = \{1.0 - [4\ (0.03)/(1.0 - 0.6)\ \pi]^{1/2}\} \times 15 = 10.4$ ksi
4. Longitudinal compression $S_{\ell 11C}$ (second of eq. (2), fig. 5)
   $S_{\ell 11C} = 10.0 \times 7.6 + 1.5 \times 10.4 = 102$ ksi
5. Longitudinal flexural strength (lower estimate equation, example 4.4)
   $S_{\ell 11F} = 3 \times 210/(1.0 + 210/102) = 206$ ksi

which is about 9 percent less than the 227 ksi value calculated without voids in example 4.4. Two points are worth noting: (1) step (4) results in a void degradation of about 13 percent in $S_{\ell 11C}$ and (2) the void degradation is more severe for the longitudinal compression strength than for the longitudinal flexural strength (13 percent versus 9 percent respectively).

The above calculations show that the composite micromechanics equations in figure 6 and the alternates in Examples 4.4 and 4.5 can be used to obtain reasonable estimates for through-the-thickness uniaxial strengths. The calculations also show that the equations can be used to interpret measured data. In either case, these equations should be used judiciously.

UNIAXIAL FRACTURE "TOUGHNESS"

Fracture toughness is a measure of a material to resist defects such as holes, slits and notches. Fracture toughness is described by fracture toughness parameters associated with distinct fracture modes (ref. 7). Three fracture modes are generally considered: opening mode (Mode I), in-plane shear (Mode II) and out-of-plane shear (Mode III). In the case of unidirectional composites and assuming full thickness penetration defects, there are three major in-plane fracture toughness parameters herein defined as: (1) longitudinal fracture toughness ($\mathcal{J}_{\ell 11T}$); (2) transverse fracture toughness ($\mathcal{J}_{\ell 22T}$); and (3) in-plane (intralaminar) shear fracture toughness ($\mathcal{J}_{\ell 12S}$). These three are parallel to the uniaxial in-plane strengths $S_{\ell 11T}$, $S_{\ell 22T}$ and $S_{\ell 12S}$, respectively. These fracture toughness parameters are used herein to denote far-field stress required to produce additional damage in the composite. It is not clear whether far field shear stress will produce Mode II fracture in unidirectional composites or some component of Mode I (opening) fracture. In view of this we consider only Mode I, opening fracture modes $\ell 11T$ and $\ell 22T$.

The equations describing the longitudinal and transverse fracture toughness parameters ($\mathcal{J}_{\ell 11T}$ and $\mathcal{J}_{\ell 22T}$) are given in figure 7 (ref. 8) with attendant schematics. Two sets of equations are given. In the first set (eq. (1) and (2)), $\ell 11T$ and $\ell 22T$ are expressed in terms of ply properties while in the second set (eq. (3) and (4)) they are expressed in terms of constituent properties. It can be seen in Eqs. (3) and (4) that: (1) $\mathcal{J}_{\ell 11T}$ depends linearly on S_{fT} and depends in a complex way on K_f, (E_{f11}/E_m), (E_m/E_{f22}), (G_m/G_{f12}) and ν_m; and (2) $\mathcal{J}_{\ell 22T}$ depends linearly on S_{mT} and in a complex way on the other constituent material properties. Examining only key parameters k_f, E_{f11}, E_m, S_{fT} and S_{mT}, $\mathcal{J}_{\ell 11T}$ increases with increasing k_f, E_{f11}, E_m and with decreasing E_{f11},

while $\mathscr{d}_{\ell 22T}$ increases with increasing E_{f11}, S_{mT} and with decreasing k_f and E_m. Equations (3) and (4), figure 7, are cumbersome to use. It is easier to use equation (1) and (2), figure 7, in conjunction with the ply mechanical properties equations summarized in figure 8. Two examples below illustrate use of these equations and interpretation of the results.

Example 5.1. Calculate the longitudinal fracture toughness of an AS/E (IMHS) composite with 0.6 fiber volume ratio. This is accomplished using the following steps together with equations from figures 7 and 8, and respective constituent properties from tables 1 and 2.

1. Calculate $S_{\ell 11T}$ (eq. (1), fig. 5)
   $S_{\ell 11T} = 0.6 \times 350 = 210$ ksi
2. Calculate $E_{\ell 11}$ (first equation, fig. 8)
   $E_{\ell 11} = 0.6 \times 31 + 0.4 \times 0.5 = 18.8$ mpsi
3. Calculate $E_{\ell 22}$ (second equation, fig. 8)
   $E_{\ell 22} = 0.5/[1.0 - \sqrt{0.6}(1.0-0.5/2.0)] = 1.2$ mpsi
4. Calculate ν_{12} (fifth equation, fig. 8)
   $\nu_{\ell 12} = 0.6 \times 0.20 + 0.4 \times 0.35 = 0.26$
5. Calculate $G_{\ell 12}$ (third equation, fig. 8)
   $G_{\ell 12} = 0.185/[1.0 - \sqrt{0.6}(1-0.185/2.0)] = 0.62$ mpsi
6. Calculate $\mathscr{d}_{\ell 11T}$ (eq. (1), fig. 7)
   $\mathscr{d}_{\ell 11T} = 210/\{1.0 + [2\,(18.8/1.2 - 0.26) + (18.8/0.62)]^{1/2}\} = 24$ ksi

This implies that the far-field (P/A-type) ply stress will be 24 ksi when the crack-like defect starts growing. This can also be interpreted as follows: The stress required to produce additional damage is reduced by a factor of about ten compared to that in a ply without defects.

Example 5.2. Calculate the transverse fracture toughness ($\mathscr{d}_{\ell 22T}$) in an AS/E (IMHS) composite with 0.6 fiber volume ratio. This is calculated using appropriate equations figures 7 and 8, respective properties from Tables 1 and 2 and the following steps.

1. Calculate $E_{\ell 11}$. From example 5.1 step 2, $E_{\ell 11} = 18.8$ mpsi
2. Calculate $S_{\ell 22T}$ (eq. (3), fig. 5) with partial interfacial bond.
   a. $S_{mT} = \{1.0 - [4\,(0.05)/(1.0 - 0.6)\,\pi]^{1/2}\}\ 15 = 9.0$ ksi
   b. $S_{\ell 11T} = [1.0 - (\sqrt{0.6} - 0.6)\,(1.0 - 0.5/2.0)] \times 9.0 = 7.8$ ksi
3. Calculate $E_{\ell 22}$. From example 5.1, step 3, $E_{\ell 22} = 1.2$ mpsi
4. Calculate $\nu_{\ell 12}$. From example 5.1, step 4, $\nu_{\ell 12} = 0.26$
5. Calculate $G_{\ell 12}$. From example 5.1, step 5, $G_{\ell 12} = 0.62$ mpsi
6. Calculate $\mathscr{d}_{\ell 22T}$. From equation (2), figure 7

$$\mathscr{d}_{\ell 22T} = 7.8/\left\{1.0 + (1.2/18.8)^{1/2}\,[2\,(1.0 - 0.26) + 18.8/0.62]^{1/2}\right\} = 3.2 \text{ ksi}$$

This implies that the far-field (P/A-type) ply stress will be 3.2 ksi when additional damage in the vicinity of the defect will occur. Or alternatively, the stress required to produce additional damage is reduced by a factor of about 2.5 compared to that in a ply without defects. It is worth noting that this relatively low value of 3.2 ksi required to produce additional damage is a major contributor to the brittle-like strength behavior transverse to the fiber direction.

UNIAXIAL IMPACT RESISTANCE--IN-PLANE

Uniaxial impact resistance of unidirectional composites is defined herein as an in-plane uniaxial impact energy density. It is denoted by the generic symbol $\mathscr{X}_{\ell}$ and is associated with a corresponding in-plane uniaxial impact stress. There are five impact energy densities: (1) longitudinal tension ($\mathscr{X}_{\ell 11T}$); (2) longitudinal compression ($\mathscr{X}_{\ell 11C}$); (3) transverse tension ($\mathscr{X}_{\ell 22T}$); (4) transverse compression ($\mathscr{X}_{\ell 22C}$) and intralaminar shear ($\mathscr{X}_{\ell 12S}$). The composite micromechanics equations for these impact energy densities are summarized in figure 9 with attendant schematics. The wiggly arrows in the schematics denote dynamic stresses. These equations are derived by assuming linear stress-strain behavior to fracture (fig. 3) under dynamic stress. The first five equations describe the five in-plane uniaxial impact energy densities while the last equation describe the void degradation effect as mentioned previously.

The following are observed from the equations in figure 9: (1) $\mathscr{X}_{\ell 11T}$ varies linearly with k_f, quadratically with S_{fC} and inversely with E_{f11}; (2) $\mathscr{X}_{\ell 11C}$ also varies linearly with k_f, quadratically with S_{fC} (assuming fiber compressive fracture) and inversely with E_{f11}; (3) $\mathscr{X}_{\ell 22T}$ decreases nonlinearly with k_f, increases quadratically with S_{mT}, decreases inversely with E_m, and increases nonlinearly with increasing ratio (E_m/E_{f22}); (4) $\mathscr{X}_{\ell 22C}$, and $\mathscr{X}_{\ell 12S}$ are matrix dominated; and (6) the matrix dominated impact energy densities decrease nonlinearly with increasing void content. Several examples below illustrate use of the equations in figure 9.

Example 6.1. Calculate the longitudinal tensile impact energy density for an AS/E (IMHS) unidirectional composite with 0.6 fiber volume ratio. Using respective properties from table 1 and $k_f = 0.6$ in equation 1, figure 9.

$\mathscr{X}_{\ell 11T} = 0.6 \times 350\ 000^2/2 \times 31\ 000\ 000 = 1185$ (lb/sq in.)/cu in.

Example 6.2. Calculate the longitudinal compressive impact energy density for an AS/E (IMHS) unidirectional composite with 0.6 fiber volume ratio. Using S_{fC} $0.9S_{fT}$, $S_{fT} = 350$ ksi, $E_{f11} = 31$ mpsi and $k_f = 0.6$ in equation 2, figure 9.

$\mathscr{X}_{\ell 11C} = 0.6 \times (0.9 \times 350\ 000)^2/2 \times 31\ 000\ 000 = 960$ (lb/sq in./cu in.)

It is instructive to calculate $\mathscr{X}_{\ell 11C}$ assuming delamination/shear fracture mode (example 3.2). For this case $\mathscr{X}_{\ell 1C} = 370$ (lb/sq in.)/cu in. or a decrease of about 61 percent.

Example 6.3. Calculate the transverse tensile impact energy density ($\mathscr{X}_{\ell 22T}$) for an AS/E (IMHS) unidirectional composite with 0.6 fiber volume ratio. Using respective property values from tables 1 and 2 and $k_f = 0.6$ in equation 3, figure 9 and degrading S_{mT} for incomplete interfacial bond (example 3.3)

$$S_{mT} = \left\{1.0 - (4\,(0.05)/(1.0 - 0.6)\,\pi]^{1/2}\right\}\ 15 = 9 \text{ ksi}$$

$$\mathscr{X}_{\ell 22T} = [1.0 - (\sqrt{0.6} - 0.6)\,(1.0 - 0.5/2.0)]^2 \times [1.0 - \sqrt{0.6}\,(1.0 - 0.5/2.0)] \times 9000^2/2 \times 500\ 000$$

$$= 26 \text{ (lb/sq in.)/cu in.}$$

This value is about 2 percent of the longitudinal tensile (1185 (lb/sq in.)/cu in., example 6.1) and illustrates the fragile nature of unidirectional composites when subjected to transverse loads.

Example 6.4. Calculate the transverse compressive impact energy density for an AS/E (IMHS) unidirectional composite with 0.6 fiber volume ratio. Recall that incomplete bond does not degrade the transverse compressive behavior (example 3.4). Using respective property values from tables 1 and 2 and $k_f = 0.6$ in equation (4), figure 9

$$\mathscr{X}_{\ell 22c} = [1.0 - (\sqrt{0.6} - 0.6)(1.0 - 0.5/2.0)]^2 \times [1.0 - 0.6(1-0.5/2.0)] \times 35\,000^2/2 \times 500\,000 = 388 \text{ (lb/sq in.)/cu in.}$$

which is about 15 times $\mathscr{X}_{\ell 22T}$ indicating substantial "tougher" behavior in transverse compression. Also $\mathscr{X}_{\ell 22C}$ is about the same as that for $\mathscr{X}_{\ell 11C}$ (370 (lb/sq/in./cu. in.) calculated by assuming delamination/shear compression fracture mode (example 6.2). This imples that longitudinal compression and transverse compression fractures probably occur simultaneously during normal impact.

Example 6.5. Calculate the intralaminar shear energy density for an AS/E (IMHS) unidirectional composite with 0.6 fiber volume ratio. Using respective property values from tables 1 and 2 and $k_f = 0.6$ in equation (5), figure 9 and degrading S_{ms} for incomplete interfacial bond (example 3.4)

$$\mathscr{X}_{\ell 12S} = [1.0 - (\sqrt{0.6} - 0.6)(1.0 - 0.185/2.0)]^2 \times [1.0 - \sqrt{0.6}(1.0 - 0.185/2.0) \times 9700^2/2 \times 185\,000 = 53.5 \text{ (lb/sq in.)/cu in.}$$

$$S_{ms} = \left\{1.0 - [4(0.02)/(1.0 - 0.6)\pi]^{1/2}\right\} \times 13 = 9.7 \text{ ksi}$$

The effects of voids on matrix dominated impact energy densities can be calculated by degrading the matrix strength first using equation 6, figure 9 and then substituting the degraded value in the appropriate equation. See also example 3.6.

UNIAXIAL IMPACT RESISTANCE--THROUGH-THE-THICKNESS

Through-the-thickness impact resistance in unidirectional composites result from out-of-plane normal impacts. These are defined herein as impact energy densities, are denoted by the generic symbol $\mathscr{X}_\ell$ and are, respectively: (1) longitudinal interlaminar shear ($\mathscr{X}_{\ell 13S}$); (2) transverse interlaminar shear ($\mathscr{X}_{\ell 23S}$); (3) longitudinal flexure ($\mathscr{X}_{\ell 11F}$) and transverse flexure ($\mathscr{X}_{\ell 22F}$). Each of these impact energy densities is associated with a dynamic stress corresponding, respectively to: $S_{\ell 13S}$, $S_{\ell 23S}$, $S_{\ell 11F}$ and $S_{\ell 22F}$. There is also a through-the-thickness normal impact energy density. However, this impact energy density is the same as the in-plane impact energy density $\mathscr{X}_{\ell 22T}$ or $\mathscr{X}_{\ell 22C}$ described in section 6.

The composite micromechanics equations for through-the-thickness impact energy densities are summarized in figure 10 with attendant schematics. The following are observed from the equations in figure 10: (1) $\mathscr{X}_{\ell 13S}$ is the same as $\mathscr{X}_{\ell 12S}$; it decreases nonlinearly with increasing k_f, increases nonlinearly with increasing ratio (G_m/G_{f12}), it increases quadratically with S_{mS} and increases inversely as G_m decreases; (2) $\mathscr{X}_{\ell 23S}$ has about the same behavior as $\mathscr{X}_{\ell 13S}$; (3) $\mathscr{X}_{\ell 11F}$ increase linearly with k_f and quadratically with S_{fT}, and increases inversely as E_{f11} and the ratio (S_{fT}/S_{fc}) decrease; (4) $\mathscr{X}_{\ell 22F}$ decreases nonlinearly with increasing k_f and with increasing ratio E_m/E_{f22}, increases quadratically with S_{mT}, increases inversely as the square of the

(S_{mT}/S_{mc}) ratio and increases as E_m decreases. Several examples below illustrate use of the equations in figure 10.

Example 7.1. Calculate the longitudinal interlaminar shear impact energy density ($\mathscr{X}_{\ell 13S}$) for an AS/E (IMHS) unidirectional composite with 0.6 fiber volume ratio. Since $\mathscr{X}_{\ell 13S}$ is the same as $\mathscr{X}_{\ell 12S}$, (the equation for $\mathscr{X}_{\ell 13S}$ is identical to eq. 5, fig. 9) from example 6.5.
$\mathscr{X}_{\ell 13S} = \mathscr{X}_{\ell 12S} = 53.5$ (lb/sq.in./cu.in.)

Example 7.2. Calculate the transverse interlaminar shear impact energy density ($\mathscr{X}_{\ell 23S}$) for an AS/E (IMHS) unidirectional composite with 0.6 fiber volume ratio. Using respective property values from tables 1 and 2, and $k_f = 0.6$ in equation for $\mathscr{X}_{\ell 23S}$, figure 10, and degrading S_{mS} for incomplete interfacial bond.

$$S_{mS} = \{[1.0 - [4\ (0.02)/(1.0 - 0.6)\ \pi]^{1/2}\}\ 13 = 9.7 \text{ ksi}$$

$$\mathscr{X}_{\ell 23S} = [1.0 - 0.6\ (1.0 - 0.185/1.0)]^2\ 9700^2/2 \times 185\ 000\ [1 - 0.6\ (1.0 - 0.185/1.0] = 67.7 \text{ (lb/sq in.)/cu in.}$$

It is interesting to note that for this example $\mathscr{X}_{\ell 23S}$ is about 22 percent greater than $\mathscr{X}_{\ell 13S}$. This increase is mainly due to G_{f23} which is about 50 percent of G_{f12}. Based on the relative values for $\mathscr{X}_{\ell 13S}$ and $\mathscr{X}_{\ell 23S}$ interlaminar damage will occur first due to dynamic $\sigma_{\ell 23}$.

Example 7.3. Calculate the longitudinal flexural impact energy density ($\mathscr{X}_{\ell 11F}$) for an AS/E (IMHS) unidirectional composite with 0.6 fiber volume ratio. Using respective property values from tables 1 and 2 and $k_f = 0.6$ in the equation for $\mathscr{X}_{\ell 11F}$, figure 10 (assuming $S_{fc} = 0.9\ S_{fT}$):

$$\mathscr{X}_{\ell 11F} = 4.5 \times 0.6 \times 350\ 000^2/31\ 000\ 000 \times (1.0 + 1.0/0.9)^2 = 2394 \text{ (lb/sq in.) cu in.}$$

An alternate estimate is to use $S_{\ell 11T} = 210$ ksi from example 3.1, $S_{\ell 11C} = 118$ ksi from example 3.2 and $E_{\ell 11} = 18.8$ mpsi from example 5.1 in the following equation

$$\mathscr{X}_{\ell 11F} = 4.5\ S_{\ell 11T}^2/E_{\ell 11}\ (1.0 + S_{\ell 11T}/S_{\ell 11C})^2$$

$$\mathscr{X}_{\ell 11F} = 4.5 \times 210\ 000^2/18\ 800\ 000 \times (1.0 + 210/118)^2 = 1366 \text{ (lb/sq. in.) cu. in.}$$

It is worth noting that the first estimate corresponds to $S_{\ell 11F} = 298$ ksi for fiber compression fracture; the second estimate corresponds to $S_{\ell 11F} = 227$ ksi for delamination/shear compression fracture (example 4.4). Also the second estimate is about 57 percent smaller than the first indicating that delamination/shear is a much more severe fracture mode under impact.

Example 7.4. Calculate the transverse flexural impact energy density ($\mathscr{X}_{\ell 22F}$) for an AS/E (IMHS) unidirectional composite with 0.6 fiber volume ratio. Using respective property values from tables 1 and 2, degraded S_{mT} for incomplete interfacial bond (eq. (6), fig. 9, with $k_v = 0.05$) and $k_f = 0.6$ in the equation for $\mathscr{X}_{\ell 22F}$, figure 10.

$$S_{mT} = \{1.0 - [4\ (0.05)/(1.0 - 0.6)\ \pi]^{1/2}\}\ 15 = 9.0 \text{ ksi}$$

$$\mathscr{X}_{\ell 22F} = 4.5\ [1.0 - 0.6\ (1.0 - 0.5/2.0)] \times \left[\frac{1.0 - (\sqrt{0.6} - 0.6)\ (1.0 - 0.5/2.0)}{1 + 9/35}\right]^2 \times (9000^2/500\ 000) = 146 \text{ (lb/sq in.)/cu in.}$$

It is worth noting that this value corresponds to $S_{\ell 22F}$ = 18.6 ksi which is the lower estimate in example 4.5. Also $\mathscr{X}_{\ell 22F}$ is about 10 percent of $\mathscr{X}_{\ell 11F}$, the lower estimate in example 7.3

The effect of voids on any of the through-the-thickness impact energy densities is determined by degrading S_{mT} or S_{mS} first using equation 6, figure 9 and then substituting this degraded S_m value in the applicable equation, figure 10. The remaining steps are identical to Examples 7.1 to 7.4.

ENVIRONMENTAL EFFECTS

Environmental effects refer to the effects caused by the presence of moisture and temperature in composites. The combined effects are usually called hygrothermal effects. Hygrothermal effects influence all resin-dominated properties; uniaxial strengths, fracture toughness and impact resistance. Hygrothermal effects are estimated using an empirical expression (ref. 9). The empirical expression and the rotation used are summarized in figure 11. Its application to uniaxial composite strengths and strength related properties is illustrated using the following examples.

Example 8.1. Calculate the hygrothermal effects on the ply transverse strength assuming AS/E (IMHS) unidirectional composite, k_f = 0.6, T = 270° F, T = 70° F and 1 percent moisture by weight. Several steps are required for this calculation:

1. Tgd = 420° F table 2
2. Tgw $[0.005\ (1)^2 - 0.1\ (1) + 1.0]\ 420 = 380°$ F
3. Hygrothermal degradation ratio (P_{HTM}/P_O) for resin-dominated properties is
   $P_{HTM}/P_O = [(380-270)/(420-70)]^{1/2} = 0.56$

This means that all resin dependent properties E_m, G_m and S_m must be reduced by this ratio prior to their use in the applicable equation.

4. The reduced matrix properties (table 2) are
   $S_{mT} = 0.56 \times 15 = 8.4$ ksi
   $E_m = 0.56 \times 0.5 = 0.28$ mpsi
5. Degrade S_{mT} for partial interfacial bond assuming 5 percent voids by volume
   $S_{mT} = \{1.0 - [4.(0.05)/(1 - 0.6)\ \pi]^{1/2}\}8.4 = 5.0$ ksi
6. Using equation 3, figure 5 with the respective degraded properties
   $S_{\ell 22T} = [1.0 - (\sqrt{0.6} - 0.6)\ (1.0 - 0.25/2.0)]\ 5.0 = 4.2$ ksi

which is a decrease of 46 percent compared to room temperature dry 7.8 ksi (example 3.3). Obviously, this is severe degradation of the hygrothermal environment assumed in the example. It is important to note that the ratio of environmentally degraded to room-temperature dry (4.2/7.8) = 0.53 which is very close to 0.56 predicted in step 3 above. This indicates that the hygrothermal degradation ratio can be applied to either (1) resin or (2) resin-dominated composite properties equally well (ref. 9). It is recommended to use the glass transition temperature of the composite for the second case. The glass transition temperature of the composite is about 50° F greater than that of the resin.

Example 8.2. Calculate the transverse flexural strength for the same composite and environmental conditions as in example 8.1. Again several steps are required

1. From example 8.1, step 3
   $P_{HTM}/P_o = 0.56$
   from which follows: $S_{mC} = 0.56 \times 35 = 19.6$ ksi and
   $E_m = 0.28$ mpsi
2. The transverse compression stress is
   $S_{\ell 22C} = [1.0 - (\sqrt{0.6} - 0.6)(1.0 - 0.28/2.0)]\ 19.6 = 16.7$ ksi
3. Using $S_{\ell 22C} = 16.7$ ksi and $S_{\ell 22T} = 4.2$ ksi (example 8.1, step 6) in the lower estimate equation (example 4.5).
   $S_{\ell 22F} = 3 \times 4.2/(1.0 + 4.2/16.7) = 10.1$ ksi

which is about 0.54 of 18.6 ksi, the room temperature dry value calculated in example 4.5. This calculation also illustrates that the hygrothermal degradation can be applied to a resin-dominated composite property.

Example 8.3. Calculate the transverse fracture toughness ($\mathcal{J}_{\ell 22T}$) for the composite and hygrothermal environment in example 8.1. The procedure for this calculation is the same as that in example 5.2.

1. Using the $(P_{HTM}/P_o) = 0.56$ in the equations for $E_{\ell 22}$ and $G_{\ell 12}$, figure 8.
   $E_{\ell 22} = 0.28/[1.0 - \sqrt{0.6}(1.0 - 0.28/2.0)] = 0.839$ mpsi
   $G_{\ell 12} = 0.103/[1.0 - \sqrt{0.6}(1.0 - 0.103/2.0)] = 0.39$ mpsi
2. $E_{\ell 11}$ and $\nu_{\ell 12}$ remain practically unchanged.
   $E_{\ell 11} = 18.7$ and $\nu_{\ell 12} = 0.26$ (example 5.1, steps 2 and 4)
3. $S_{\ell 22T} = 4.2$ ksi (example 8.1, step 6)
4. Substituting respective values from steps 1, 2, and 3 in equation 2, figure 7

$$\mathcal{J}_{\ell 22T} = 4.2/1.0 + (0.84/18.7)^{1/2} \times [2(1.0 - 0.26) + 18.7/0.39]^{1/2} = 1.7 \text{ ksi}$$

which is about 0.53 of the value calculated in example 5.2. Even in this complex expression the environment degrades the composite resin dominated property in about the same ratio as the resin property.

Example 8.4. Calculate the transverse impact energy density ($\mathcal{K}_{\ell 22T}$) for the composite and environmental conditions in example 8.1. The procedure for this calculation is the same as that in example 6.3.

1. The degraded properties needed for equation 3, figure 9 are
   $E_m = 0.28$ mpsi (example 8.1, step 4 and $S_{mT} = 5.0$ ksi (example 8.1, step 5).
2. Using respective values in equation 3, figure 9
   $$\mathcal{K}_{\ell 22T} = [1.0 - (\sqrt{0.6} - 0.6)(1.0 - 0.28/2.0)]^2 \times [1.0 - \sqrt{0.6}(1.0 - 0.28/2.0)] \times 5000^2/2 \times 280\,000 = 10.8 \text{ (lb/sq. in.) cu. in.}$$

which is about 42 percent of 26 (lb/sq in.)/cu in., in the room temperature dry value in example 6.3. This ratio corresponds to a decrease of about equal to the hygrothermal degradation ratio raised to the 3/2 power or $(0.56)^{3/2}$. Indicating again that resin dominated composite properties

degrade in the same ratio as the resin when subjected to hygrothermal environments.

GENERAL DISCUSSION

The several examples presented illustrate the usefulness and advantage of having a unified set of micromechanics equations summarized in Figs. 5 to 11 for the strength, fracture toughness and impact resistance of composites. The examples also illustrate how the various strengths and other mechanical properties are interrelated. In addition, they provide detailed and quantitative insight into the micromechanic strength behavior of composites. Furthermore, the various equations can be selectively used to conduct parametric studies as well as sensitivity analyses to assess acceptable ranges of various constituent material and environmental factors.

Limited comparisons were provided between predicted values and available measured data for some of the numerical examples. It is important to note that the primary purpose of this report is to describe a unified set of simple, working equations and illustrate its versatility with a variety of numerical examples. These examples demonstrate computational effectiveness and illustrate interrelationships of various strengths and other properties at the micromechanistic level. It is highly recommended that the reader use this unified set of micromechanics equations to predict various properties of interest to him and compare them with measured data or with known values. This provides a direct approach to assess the application and limitations of these equations as well as guidelines on how to modify them.

Another important aspect of having this unified set of micromechanics strength equations is that they can be used to plan and guide experimental programs for maximum benefit with minimum testing. These micromechanics equations can be advantageous in a number of other ways. Many of these other ways become "self evident" after some familiarity has been obtained.

The two tables summarizing constituent material properties illustrate the amount of data needed for effective use of a unified set of micromechanics equations. The data in these tables were compiled from many sources and many values are estimates which were inferred from predicted results and curve fits. The data are included for three main reasons: (1) to illustrate that the micromechanics equations need numerous properties; (2) to bring attention to the fact that many of these properties have not been measured and, hopefully, to stimulate enough interest to develop experimental methods to measure them; and (3) to provide indicative ranges of properties of both fibers and matrices. It cannot be overemphasized that the data should be considered dynamic in the sense that they should be continuously modified if better values are known or become available.

Lastly, the unified set of micromechanics equations described herein, in conjunction with classical laminate theories and combined stress failure criteria can be used to calculate laminate strength based on first ply failure.

CONCLUSIONS

A unified set of composite micromechanics equations of simple form is summarized and described. This unified set includes composite micromechanics equations for predicting (1) ply in-plane uniaxial strength; (2) through-the-thickness strength (interlaminar and flexural); (3) in-plane fracture toughness; (4) in-plane impact resistance; and (5) through-the-thickness (interlaminar and flexural) impact resistance. Equations are also included for predicting the hygrothermal effects on strength, fracture toughness and impact resistance. Several numerical examples are worked out to illustrate the ease of use of the various composite micromechanics equations. The numerical examples were selected, in part, to demonstrate the interrelationship of the various constituent properties in composite strength and strength related behavior, and also to provide comparisons with available experimental data. This unified set of micromechanics equations makes it possible and cost-effective to assess composite strength, "fracture toughness", impact resistance and attendant environmental effects for preliminary designs of composite structures.

REFERENCES

1. C. C. Chamis, "Micromechanics Strength Theories", Fracture and Fatigue, L. J. Brautman, Ed., Academic Press, 1974, pp. 94-148.

2. W. J. Renton, Ed., Hybrid and Select Metal Matrix Composites: A State-of-The-Art Review, American Institute of Aeronautics and Astronautics, 1977, pp. 15-16.

3. C. C. Chamis and J. H. Sinclair, "Prediction of Composite Hygral Behavior Made Simple", Proceedings of the Thirty-Seventh Annual Conference of the Society of Plastics Industry (SPI) Reinforced Plastics/Composites Institute, 1982.

4. L. A. Friedrich and J. L. Preston, Jr., "Impact Resistance of Fiber Composite Blades Used in Aircraft Turbine Engines", PWA-4727, Pratt & Whitney Aircraft, East Hartford, CT., NASA CR-134502, May 1973.

5. C. C. Chamis, R. F. Lark and J. H. Sinclair, "Mechanical Property Characterization of Intraply Hybrid Composites", Test Methods and Design Allowables for Fibrous Composites, ASTM STP-734, C. C. Chamis, Ed., American Society for Testing and Materials, 1981, pp. 261-280.

6. J. H. Sinclair and C. C. Chamis, "Compression Behavior of Unidirectional Fibrous Composite", NASA TM 82833, 1982.

7. P. C. Paris and G. C. Sih, "Stress Analysis of Cracks", Fracture Toughness Testing and Its Applications, ASTM STP 381, American Society for Testing and Materials, 1965, pp. 30-83.

8. C. C. Chamis and G. T. Smith, "Resin Selection Criteria for Tough Composite Structures", NASA TM 83449, 1983.

9. C. C. Chamis, R. F. Lark and J. H. Sinclair, "Integrated Theory for Predicting the Hygrothermomechanical Response of Advanced Composite Structures", Advanced Composite Materials Environmental Effects, ASTM STP-658, J. R. Vinson, Ed., American Society for Testing and Materials, 1978, pp. 160-192.

TABLE I. - FIBER PROPERTIES[a]

Name	Symbol	Units	Boron	HMS	AS	T300	KEV	S-G	E-G
Number of fibers/end	N_f	----------	1	10 000	10 000	3000	580	204	204
Fiber diameter	d_f	in.	0.0056	0.0003	0.0003	0.0003	0.00046	0.00036	0.00036
Density	ρ_f	lb/in.^{3}	0.095	0.070	0.063	0.064	0.053	0.090	0.090
Longit. modulus	E_{f11}	10^6 psi	58	55.0	31.0	32.0	22	12.4	10.6
Transv. modulus	E_{f22}	10^6 psi	58	0.90	2.0	2.0	0.6	12.4	10.6
Long. shear modulus	G_{f12}	10^6 psi	24.2	1.1	2.0	1.3	0.42	5.17	4.37
Transv. shear modulus	G_{f23}	10^6 psi	24.2	0.7	1.0	0.7	0.22	5.17	4.37
Long. Poisson's ratio	ν_{f12}	----------	0.20	0.20	0.20	0.20	0.35	0.20	0.22
Transv. Poisson's ratio	ν_{f23}	----------	0.20	0.25	0.25	0.25	0.35	0.20	0.22
Heat capacity	C_f	btu/lb/°F	0.31	0.20	0.20	0.22	0.25	0.17	0.17
Long. heat cond.	K_{f11}	btu/hr/ft^2/°F/in.	22	580	580	580	1.7	21	7.5
Transv. heat cond.	K_{f22}	btu/hr/ft^2/°F/in.	22	58	58	58	1.7	21	7.5
Long. th. exp. coef.	α_{f11}	10^{-6} in./in./°F	2.8	-0.55	-0.55	0.55	-2.2	2.8	2.8
Transv. th. exp. coef.	α_{f22}	10^{-6} in./in./°F	2.8	5.6	5.6	5.6	30	2.8	2.8
Long. tensile strength	S_{ft}	ksi	600	250	350	350	400	600	400
Long. compression str.	S_{fc}	ksi	700	200	260	300	75	-------	-------
Shear strength	S_{fs}	ksi	100	------	------	------	-------	-------	-------

[a]Transverse, shear, and compression properties are estimates inferred from corresponding composite properties.

TABLE II. - MATRIX PROPERTIES

Name	Symbol	Units	LM	IMLS	IMHS	HM	Poly imide	PMR
Density	ρ_m	lb/in.^{3}	0.042	0.046	0.044	0.045	0.044	0.044
Modulus	E_m	10^6 psi	0.32	0.50	0.50	0.75	0.50	0.47
Shear modulus	G_m	10^6 psi	-----	-----	-----	-----	-----	-----
Poisson's ratio	ν_m	---------	0.43	0.41	0.35	0.35	0.35	0.36
Heat capacity	C_m	Btu/lb/°F	0.25	0.25	0.25	0.25	0.25	0.25
Heat conductivity	K_m	Btu/hr/ft^2/°F/in.	1.25	1.25	1.25	1.25	1.25	1.25
Thermal exp. coef.	α_m	10^{-6} in./in./°F	57	57	36	40	20	28
Diffusivity	D_m	10^{-10} in^2/sec	0.6	0.6	0.6	0.6	0.6	0.6
Moisture exp. coef.	β_m	in./in./M	0.33	0.33	0.33	0.33	0.33	0.33
Tensile strength	S_{mt}	ksi	8	7	15	20	15	8
Compression strength	S_{mc}	ksi	15	21	35	50	30	16
Shear strength	S_{ms}	ksi	8	7	13	15	13	8
Tensile fracture strain	ϵ_{mt}	in./in. (%)	8.1	1.4	2.0	2.0	2.0	2.0
Compr. fracture strain	ϵ_{mc}	in./in. (%)	15	4.2	5.0	5.0	4.0	3.5
Shear fracture strain	ϵ_{ms}	in./in. (%)	10	3.2	3.5	4.0	3.5	5.0
Air heat conductivity	K_v	Btu/hr/ft^2/°F/in.	0.225	0.225	0.225	0.225	0.225	0.225
Glass trans. temp. (dry)	T_{GD}	°F	350	420	420	420	700	700

Notes: LM - low modulus; IMLS - intermediate modulus low strength; IMHS - intermediate modulus high strength; HM - high modulus.

Thermal, hygral, compression and shear properties aree estimates only; $G_m = E_m/2\ (1 + \nu_m)$.

TABLE III. - TYPICAL EXPERIMENTAL VALUES FOR UNIDIRECTIONAL COMPOSITE (PLY) UNIAXIAL STRENGTHS[(a)] (KSI)

Fiber	Epoxy	Fiber volume ratio	Longitudinal		Transverse		In-plane shear	Flexural		Inter-laminar shear
			tension	compres.	tension	compres.		Long.	Trans.	
Boron	505	0.50	230	360	9.1	35.0	12.0	350	40	16.0
AS	3501	.60	210	170	7.0	36.0	9.0	230	18	14.0
HMS	934	.60	120	90	6.7	28.5	6.5	150	[(b)]7	10.5
T-300	5208	.60	210	210	6.5	36.0	9.0	260	18	14.0
KEVLAR-49	-----	.60	200	40	4.0	9.4	8.7	90	6	7.0
GLASS										
S (901-S)	1002S	.60	220	120	6.7	25.0	12.0	320	21	14.0
E	1002	.60	160	90	4.0	20.0	12.0	165	20	14.0

(a)Data in this table was compiled from refs. 2, 3, 4, 5.
(b)Estimate.

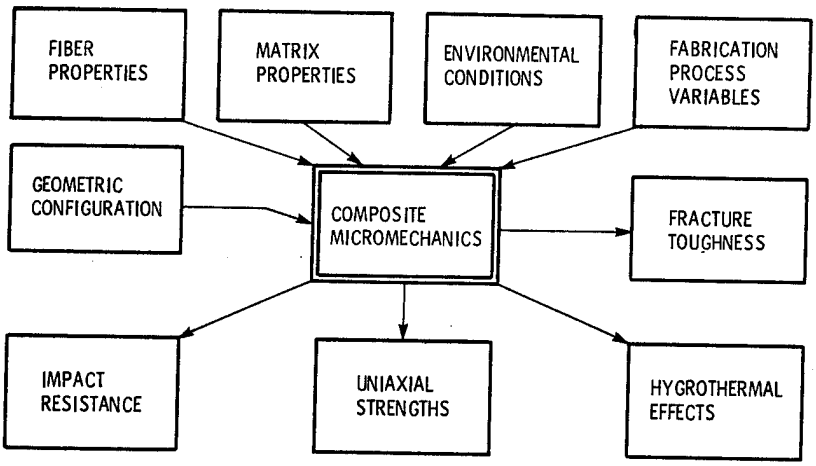

Figure 1. - Concepts, math-models and equations used to predict unidirectional composite (ply) uniaxial strengths from constituent material properties, geometric configuration, fabrication process variables and environmental conditions.

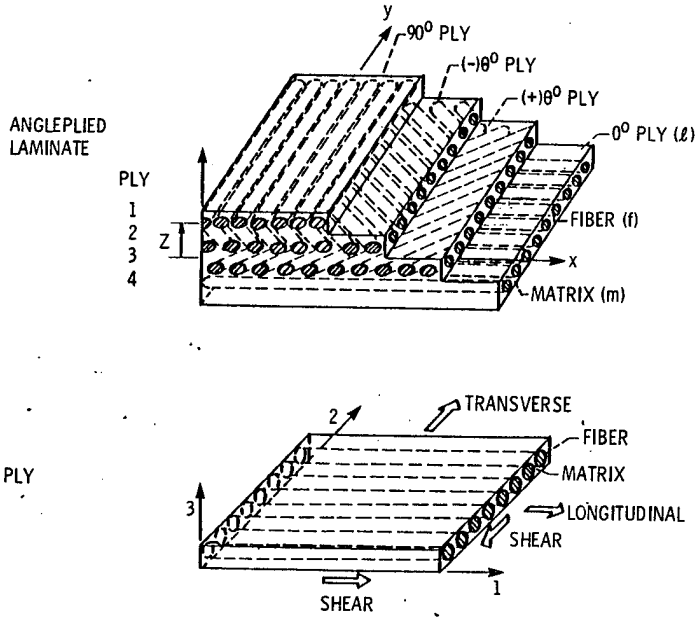

Figure 2. - Typical fiber composite geometry.

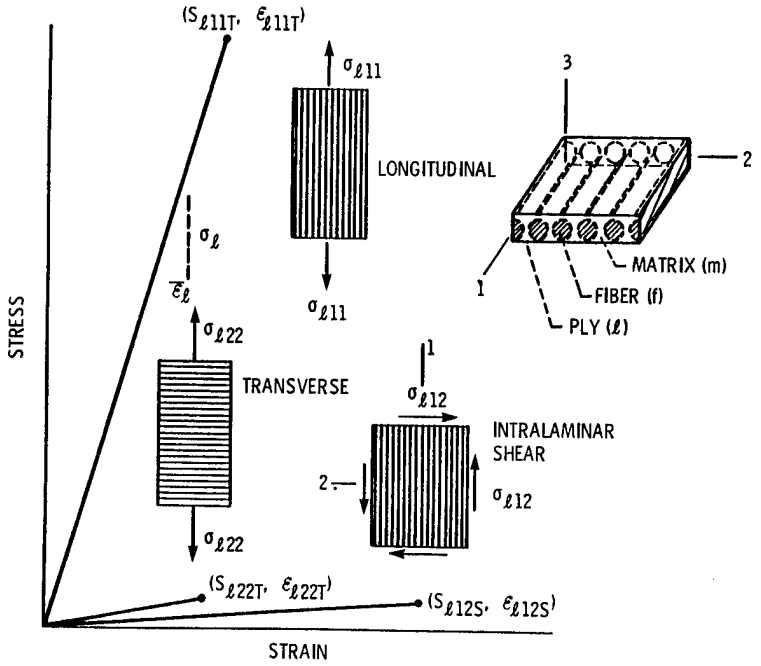

Figure 3. - Typical stress-strain behavior of unidirectional fiber composites.

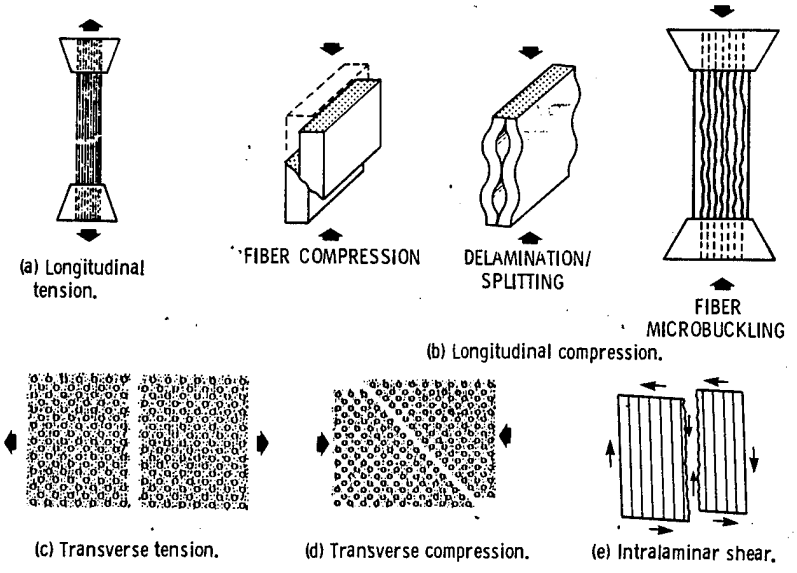

Figure 4. - In-plane fracture modes of unidirectional (ply) fiber composites.

1. LONGITUDINAL TENSION: $S_{\ell 11T} \approx k_f S_{fT}$

2. LONGITUDINAL COMPRESSION:

FIBER COMPRESSION: $S_{\ell 11C} \approx k_f S_{fC}$

DELAMINATION/SHEAR: $S_{\ell 11C} \approx 10 S_{\ell 12S} + 2.5 S_{mT}$

MICROBUCKLING: $S_{\ell 11C} \approx \dfrac{G_m}{1 - k_f\left(1 - \dfrac{G_m}{G_{f12}}\right)}$

3. TRANSVERSE TENSION: $S_{\ell 22T} \approx \left[1 - (\sqrt{k_f} - k_f)(1 - E_m/E_{f22})\right] S_{mT}$

4. TRANSVERSE COMPRESSION: $S_{\ell 22C} \approx \left[1 - (\sqrt{k_f} - k_f)(1 - E_m/E_{f22})\right] S_{mC}$

5. INTRALAMINAR SHEAR: $S_{\ell 12S} \approx \left[1 - (\sqrt{k_f} - k_f)(1 - G_m/G_{f12})\right] S_{mS}$

6. FOR VOIDS: $S_m \approx \left\{1 - \left[4k_v/(1 - k_f)\pi\right]^{1/2}\right\} S_m$

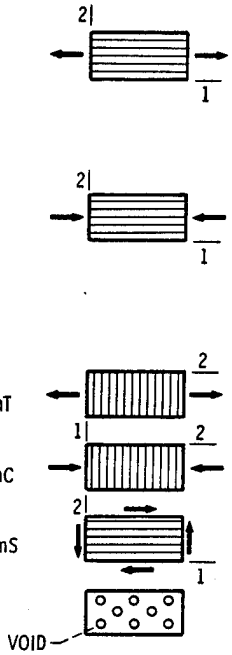

Figure 5. - Composite micromechanics: uniaxial strengths - in-plane.

1. INTERLAMINAR SHEAR: $S_{\ell 13S} \approx \left[1 - (\sqrt{k_f} - k_f)(1 - G_m/G_{f12})\right] S_{mS}$

$S_{\ell 23S} \approx \left[\dfrac{1 - \sqrt{k_f}(1 - G_m/G_{f23})}{1 - k_f(1 - G_m/G_{f23})}\right] S_{mS}$

2. SHORT: BEAM: SHEAR $S_{\ell 13SB} \approx 1.5\, S_{\ell 13S}$

$S_{\ell 23SB} \approx 1.5\, S_{\ell 23S}$

3. FLEXURAL: $S_{\ell 11F} \approx \dfrac{3 k_f S_{fT}}{1 + \dfrac{S_{fT}}{S_{fC}}}$

$S_{\ell 22F} \approx \dfrac{3\left[1 - (\sqrt{k_f} - k_f)(1 - E_m/E_{f22})\right] S_{mT}}{1 + \dfrac{S_{mT}}{S_{mC}}}$

4. FOR VOIDS: $S_m \approx \left\{1 - \left[4k_v/(1 - k_f)\pi\right]^{1/2}\right\} S_m$

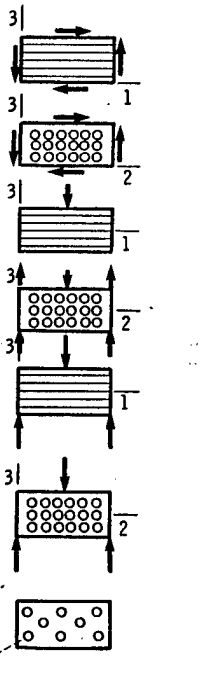

Figure 6. - Composite micromechanics: uniaxial strengths - through-the-thickness.

USING PLY PROPERTIES:

1. $$\mathcal{S}_{\ell 11T} = \frac{S_{\ell 11T}}{1 + \left[2\left(\frac{E_{\ell 11}}{E_{\ell 22}} - \nu_{\ell 12}\right) + \frac{E_{\ell 11}}{G_{\ell 12}}\right]^{1/2}}$$

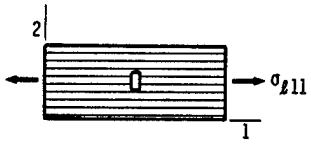

2. $$\mathcal{S}_{\ell 22T} = \frac{S_{\ell 22T}}{1 + \left(\frac{E_{\ell 22}}{E_{\ell 11}}\right)^{1/2}\left[2\left(1 - \nu_{\ell 12}\right) + \frac{E_{\ell 11}}{G_{\ell 12}}\right]^{1/2}}$$

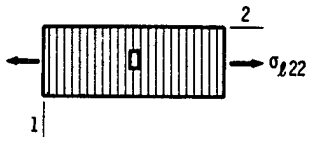

USING CONSTITUENT PROPERTIES:

3. $$\mathcal{S}_{\ell 11T} \approx \frac{k_f S_{fT}}{1 + (2 k_f E_{f11}/E_m)^{1/2}\left\{2(1 - \sqrt{k_f}) + \sqrt{k_f}\left(\frac{E_m}{E_{f22}} + \frac{G_m}{G_{f12}}\right) + \nu_m\left[1 - \sqrt{k_f}\left(1 - \frac{G_m}{G_{f12}}\right)\right]\right\}^{1/2}}$$

4. $$\mathcal{S}_{\ell 22T} = \frac{(k_f E_{f11})^{1/2}\left[1 - (\sqrt{k_f} - k_f)(1 - E_m/E_{f22})\right]\left[1 - \sqrt{k_f}(1 - E_m/E_{f22})\right]^{1/2} S_{mT}}{\left\{k_f E_{f11}\left[1 - \sqrt{k_f}(1 - E_m/E_{f22})\right]\right\}^{1/2} + \left\langle E_m\left\{2\left[1 - k_f(\nu_{f12} + \nu_m) - \nu_m\right] + k_f\left[1 - \sqrt{k_f}(1 - G_m/G_{f12})\right](E_{f11}/G_m)\right\}\right\rangle^{1/2}}$$

5. $$\mathcal{S}_{\ell 22} \approx \frac{\left[1 - \sqrt{k_f} - k_f)(1 - E_m/E_{f22})\right]\left[1 - \sqrt{k_f}(1 - E_m/E_{f22})\right]^{1/2} S_{mT}}{\left[1 - \sqrt{k_f}(1 - E_m/E_{f22})\right]^{1/2} + \left[2(1 + \nu_m)\right]^{1/2}\left[1 - \sqrt{k_f}(1 - G_m/G_{f12})\right]^{1/2}}$$

Figure 7. - Composite micromechanics: uniaxial fracture "toughness".

LONGITUDINAL MODULUS: $E_{\ell 11} = k_f E_{f11} + k_m E_m$

TRANSVERSE MODULUS: $E_{\ell 22} = \frac{E_m}{1 - \sqrt{k_f}(1 - E_m/E_{f22})} = E_{\ell 33}$

SHEAR MODULUS: $G_{\ell 12} = \frac{G_m}{1 - \sqrt{k_f}(1 - G_m/G_{f12})} = G_{\ell 13}$

SHEAR MODULUS: $G_{\ell 23} = \frac{G_m}{1 - k_f(1 - G_m/G_{f23})}$

POISSON'S RATIO: $\nu_{\ell 12} = k_f \nu_{f12} + k_m \nu_m = \nu_{\ell 13}$

POISSON'S RATIO: $\nu_{\ell 23} = k_f \nu_{f23} + k_m\left(2\nu_m - \frac{\nu_{\ell 12}}{E_{\ell 11}} E_{\ell 22}\right)$

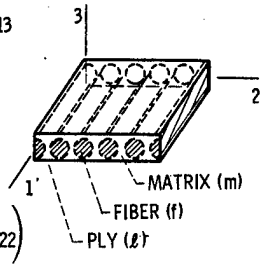

Figure 8. - Composite micromechanics, mechanical properties.

1. LONGITUDINAL TENSION: $\mathscr{E}_{\ell 11T} \approx k_f S_{fT}^2 / 2E_{f11}$

2. LONGITUDINAL COMPRESSION: $\mathscr{E}_{\ell 11C} \approx k_f S_{fC}^2 / 2E_{f11}$

3. TRANSVERSE TENSION: $\mathscr{E}_{\ell 22T} \approx \left[1 - (\sqrt{k_f} - k_f)(1 - E_m/E_{f22})\right]^2 \times \left[1 - \sqrt{k_f}(1 - E_m/E_{f22})\right] S_{mT}^2 / 2E_m$

4. TRANSVERSE COMPRESSION: $\mathscr{E}_{\ell 22C} \approx \left[1 - (\sqrt{k_f} - k_f)(1 - E_m/E_{f22})\right]^2 \times \left[1 - \sqrt{k_f}(1 - E_m/E_{f22})\right] S_{mC}^2 / 2E_m$

5. INTRALAMINAR SHEAR: $\mathscr{E}_{\ell 12S} \approx \left[1 - (\sqrt{k_f} - k_f)(1 - G_m/G_{f12})\right]^2 \times \left[1 - \sqrt{k_f}(1 - G_m/G_{f12})\right] S_{mS}^2 / 2G_m$

6. FOR VOIDS: $S_m \approx \left\{1 - \left[4 k_v / (1 - k_f)\pi\right]^{1/2}\right\} S_m$

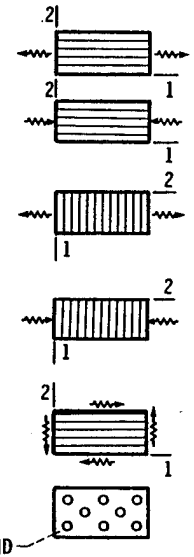

Figure 9. - Composite micromechanics: uniaxial impact resistance - in-plane. (Energy absorbed per unit volume $\mathscr{E}_\ell$.)

1. INTERLAMINAR SHEAR: $\mathscr{E}_{\ell 13S} \approx \left[1 - (\sqrt{k_f} - k_f)(1 - G_m/G_{f12})\right]^2 \times \left[1 - \sqrt{k_f}(1 - G_m/G_{f12})\right] S_{mS}^2 / 2G_m$

$$\mathscr{E}_{\ell 23S} \approx \frac{\left[1 - \sqrt{k_f}(1 - G_m/G_{f23})\right]^2 S_{mS}^2}{2G_m\left[1 - k_f(1 - G_m/G_{f23})\right]}$$

2. FLEXURAL: $$\mathscr{E}_{\ell 11F} \approx \frac{4.5\, k_f S_{fT}^2}{E_{f11}\left(1 + \frac{S_{fT}}{S_{fC}}\right)^2}$$

$$\mathscr{E}_{\ell 22F} \approx 4.5\left[1 - \sqrt{k_f}(1 - E_m/E_{f22})\right] \times \left\{\frac{\left[1 - (\sqrt{k_f} - k_f)(1 - E_m/E_{f22})\right]}{(1 + S_{mT}/S_{mC})}\right\}^2 \left(\frac{S_{mT}^2}{E_m}\right)$$

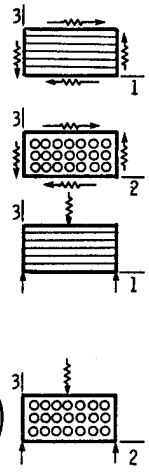

Figure 10. - Composite micromechanics: uniaxial impact resistance - through-the-thickness. (Energy absorbed per unit volume.)

GLASS TRANSITION TEMP. OF WET RESIN

$$T_{GW} = (0.005\, M_m^2 - 0.10\, M_m + 1.0)\, T_{GD}$$

EFFECTS ON MECHANICAL PROPERTIES

$$\frac{P_{HTM}}{P_O} = \left[\frac{T_{GW} - T}{T_{GW} - T_O}\right]^{1/2}$$

EFFECTS ON THERMAL PROPERTIES

$$\frac{P_{HTT}}{P_O} = \left[\frac{T_{GD} - T_O}{T_{GW} - T}\right]^{1/2}$$

GLASS TRANSITION TEMP. OF WET RESIN

$$T_{GW} = T + (T_{GD} - T_O)\,(P_{HTM}/P_O)^2$$

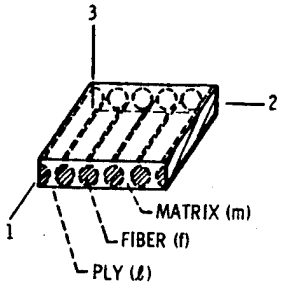

TEMPERATURE (T) ANY CONSISTANT UNITS

MOISTURE (M) WEIGHT PERCENT ($M \leq 10\%$)

SUBSCRIPTS: G = TRANSITION; D = DRY; W = WET; O = REFERENCE
HTM = HYGROTHERMAL MECHANICAL, HTT = HYGROTHERMAL THERMAL

Figure 11. - Governing equations: micromechanics - hygrothermal effects.